Journal of Magnetism and Magnetic Materials 469 (2019) 146–150

Contents lists available at ScienceDirect

Journal of Magnetism and Magnetic Materials

journal homepage: www.elsevier.com/locate/jmmm

Research articles

Coercivity enhancement and grain refinement in Nd-Fe-B sintered magnets with pyrite doping by jet milling

Fang Yang[a,*], Li You[b], Zhimeng Guo[a,*], Vladislay Paley[c], Alex A. Volinsky[c]

[a] Institute for Advanced Materials and Technology, University of Science and Technology Beijing, Beijing 100083, China
[b] State Key Laboratory for Advanced Metals and Materials, University of Science and Technology Beijing, Beijing 100083, China
[c] Department of Mechanical Engineering, University of South Florida, Tampa, FL 33620, USA

ARTICLE INFO

Keywords:
Nd-Fe-B sintered magnets
Coercivity
Pyrite
Jet milling
Grain refinement

ABSTRACT

In this paper, the methods to solve the uniformity problem of sulfur (S) element were studied in pyrite-doped Nd-Fe-B sintered magnets. With pyrite addition, the coercivity was enhanced, except for the magnets with pyrite doped by arc melting. Sulphur loss existed during the arc melting process. When pyrite doped by ball milling, the coercivity increased from 1236.3 kA/m to 1327.0 kA/m. The average grain size decreased from 9.10 μm to 7.9 μm. As a drawback, obvious sulfur clusters were formed. Jet milling was an effective way to achieve uniform distribution of S element. In the magnets with pyrite doped by jet milling, clear and continuous grain boundary phases were formed with smaller grain size. Correspondingly, the average grain size further decreased to 6.7 μm. A coercivity enhancement of 13.4% (1401.8 kA/m) was obtained with slightly decreasing in remanence and maximum magnetic energy product.

1. Introduction

Due to their excellent magnetic properties, Nd-Fe-B sintered magnets have attracted much attention in environmentally friendly applications, such as hybrid vehicles, electric vehicles, and wind power generators [1,2]. However, low coercivity is a major drawback in developing these anisotropic magnets [3]. Coercivity is an extrinsic property, which can be enhanced by increasing the anisotropy field of the $Nd_2Fe_{14}B$ phase and optimizing the microstructure [4,5]. This is commonly achieved through the introduction of heavy rare earth elements, such as Dy, to form a $(Nd, Dy)_2Fe_{14}B$ shell with higher magnetic anisotropy field at the outer region of the 2:14:1 phase grains [6]. However, due to the scarcity and high cost of Dy, there is a strong demand to reduce its usage.

Another approach aimed at enhancing coercivity is by doping non-rare earth elements to optimize microstructure by using ball milling or arc melting [7–9]. Addition of Mo, W, Nb, or V is significant to inhibit the grain growth, due to the grain boundary pinning effect [10–12]. Better wettability of the liquid phase is achieved by addition of Al, Cu, or Ga, resulting in the formation of uniform and continuous grain boundaries [13,14]. Recently, researchers have shown that sulphur (S) is beneficial for coercivity enhancement in magnets. By doping magnets with MoS_2 or WS_2, the coercivity was higher than the S-free magnets [15,16]. In the Dy/S co-doped magnets, Dy atoms in the triple junctions are avoided in the Nd_2O_2S phase, resulting in more available Dy element diffusing into the main phase. The doping method used for the S introduction is ball mixing [17,18]. As a drawback, the distribution of S element in Nd-rich phases is nonuniform, building obvious clusters.

Aiming to address the uniform distribution problem, we investigated the effects of different doping methods of S element, such as arc melting, ball milling, and jet milling. We focused our study on grain size, distribution of S element, and magnetic properties in the doped Nd-Fe-B sintered magnets. The mechanism of coercivity enhancement with S introduction by jet milling in the magnets is also discussed. To the authors' knowledge, this approach for S doping has not been reported previously.

2. Experimental procedure

Due to the low boiling point of sulfur, pyrite (FeS_2) was chosen as the raw material for obtaining the S element. The pyrite purity was greater than 99%. Three different sizes of pyrite were introduced, which were 1–5 cm, 1–3 mm, 3–5 μm, respectively. Fig. 1 shows the process flow diagram of different magnets. The Nd-Fe-B ingots, with nominal composition of 31Re(Re-Nd, Pr)-0.5Dy-bal.Fe-1.0B- 4.0 M(wt. %, M-Cu, Al, Co, Cr), were prepared by using arc melting from pure components at 1773 K under a 5×10^{-4} Pa vacuum. Each ingot was turned over three times. The ingots were separated into three parts. One

* Corresponding authors.
E-mail addresses: yangfang@ustb.edu.cn (F. Yang), guozhimengustb@163.com (Z. Guo).

https://doi.org/10.1016/j.jmmm.2018.08.057
Received 12 April 2018; Received in revised form 27 July 2018; Accepted 22 August 2018
Available online 23 August 2018

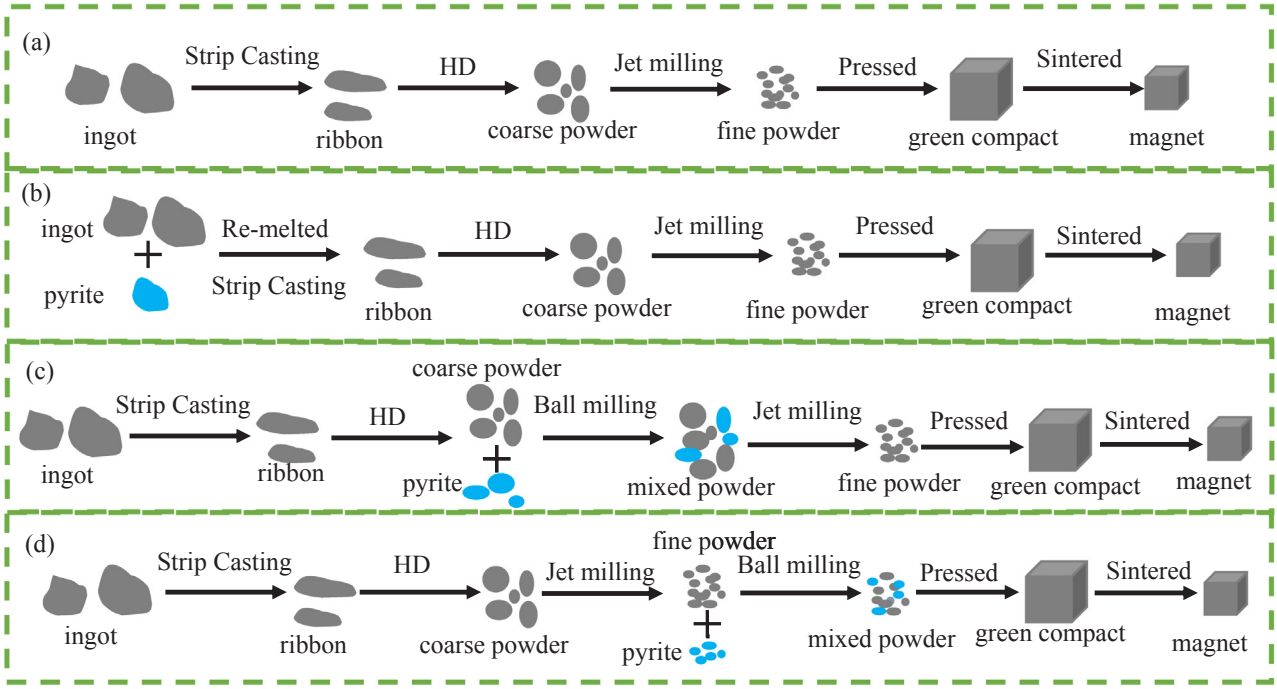

Fig. 1. The process flow diagram of: (a) undoped magnets, and S-doped magnets by (b) arc melting, (c) jet milling, and (d) ball milling.

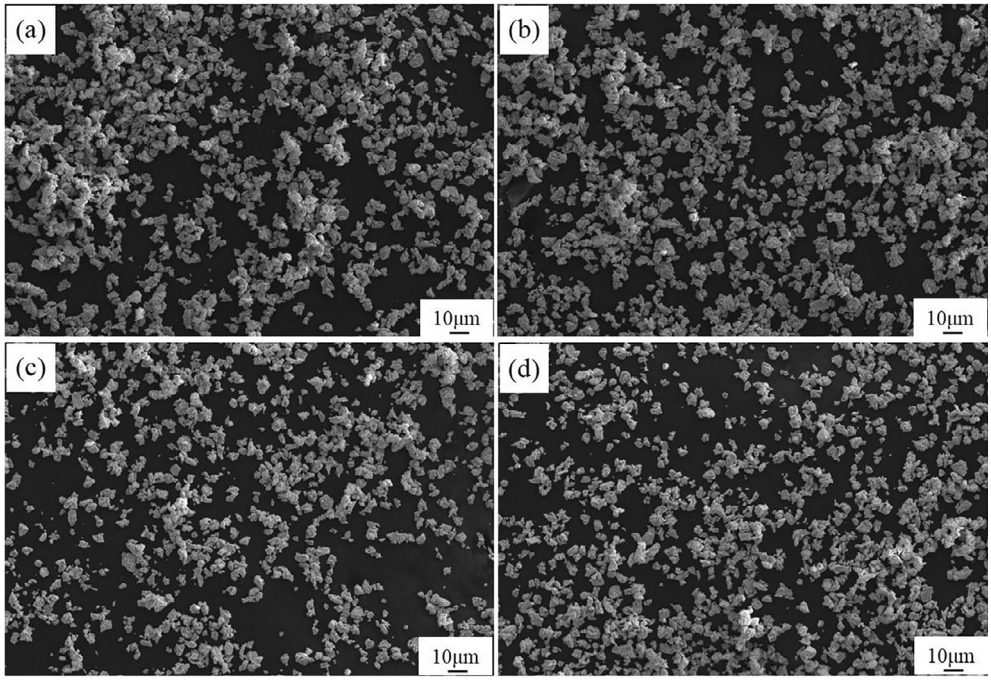

Fig. 2. The morphologies of the Nd-Fe-B powder obtained by each method of adding pyrite: (a) undoped, (b) by arc melting, (c) by jet milling, and (d) by ball milling.

part was re-melted with 0.38 wt% FeS_2 (1–5 cm). Then, the S-contained ingots were crushed to fabricate melt spun ribbons. A dynamic hydrogen decrepitation (HD) process was carried out. Then, the HD powders were crushed into finer powders by jet milling under nitrogen atmosphere, with the average particle size of 3–5 μm. The second part was crushed into powders prepared by HD followed by grinding of the ingots. The powders were mixed with 0.38 wt% FeS_2 (1–3 mm) powder by agitating with a SPEX-8000 mixer for 0.5 h. Then, the jet milling was performed. The last part was crushed to ribbons, and then a dynamic HD process was carried out on ribbons. After that, the fine powders were prepared by jet milling. Then, FeS_2 (3–5 μm) powders weighing 0.38 wt% were added to the fine powders by ball milling for 3 h. After pressing in a magnetic field of 1352 kA/m, the green compacts were vacuum-sintered at 1323 K for 3 h. Subsequently, the magnets were annealed at 1203 K for 3 h and again at 758 K for 6 h. For comparison, undoped magnets were also prepared. For the sake of distinction, the magnets with pyrite doped by arc melting, jet milling and ball milling, are called AMS, JMS, and BMS, respectively, while the S-free magnets are called CS.

The magnets were cut into cylinders of $\Phi 8 \times 5\ mm^3$ and mechanically polished. Five samples for each processing condition were tested to confirm reproducibility. Density of the sintered magnets was

determined by the Archimedes' type measurements. The room temperature magnetic properties of the processed magnets were measured by a magnetic measurement device (NIM-200C). Thermal analysis was performed using differential scanning calorimetry (DSC, NETZSCH-STA449) under a protective Ar gas. Composition of S element in magnets was determined by infrared carbon-sulfur spectrometer (EMIA-820V). Oxygen content in magnets was measured by the infrared absorption method (TCH600). Microstructural studies were conducted by backscattered electron scanning microscopy (FESEM, Supra55). Average grain sizes and grain size distributions were evaluated by an image analyzer (UTHSCSA Image Tool). Element distribution maps were obtained using electron probe microanalysis (EPMA, JEOL, JXA-8230). Phase identification were carried out at 300 kV, using transmission electron microscopy (TEM, Tecnai G2 F30 S-TWIN) combined with energy dispersive spectroscopy detector (EDS, GENESIS) and selected area electron diffraction (SAED). Thin foil specimens for the TEM analysis were prepared using an ion milling system.

3. Results and discussion

Fig. 2 shows the morphologies of the Nd-Fe-B powders obtained by different methods of doping pyrite. All the Nd-Fe-B powders have nearly similar morphologies. The average powder size is about 3–5 μm. The powder particles have an irregular shape, and a non-uniform distribution, as shown in Fig. 2.

After being sintered, all Nd-Fe-B magnets had density of approximately 7.55 g/cm^3. Fig. 3 compares the corresponding demagnetization curves for the S-free and S-doped magnets. The corresponding coercivity, H_{cj}, remanence, B_r, and maximum magnetic energy product, $(BH)_{max}$, values of the CS magnets were 1236.3 kA/m, 1.230 T, and 292.2 kJ/m^3, respectively. The magnetic properties of the AMS magnets were almost the same with the undoped magnets, as shown in Fig. 3. H_{cj} for the BMS magnets increased to 1327.0 kA/m, 7.3% higher than of the CS magnets. Meanwhile, the B_r and $(BH)_{max}$ decreased to 1.193 T and 286.1 kJ/m^3, respectively. However, H_{cj} reached its maximum value in the JMS magnets, with an increase from 1236.3 kA/m to 1401.8 kA/m, 13.4% higher than that of the CS magnets. In addition, the Br and $(BH)_{max}$ decreased to 1.198 T and 286.7 kJ/m^3, respectively. It can be inferred that the introduction of S element results in a slight decrease in Br and $(BH)_{max}$. The S element addition is beneficial to enhance the coercivity of the magnets, except in the case of AMS magnets.

The results of the composition analysis of the S and O elements in the pyrite-doped magnets are listed in Table 1. There exists a significant difference of S content in the magnets when pyrite is introduced by the different methods, whereas the O content is almost the same (nearly

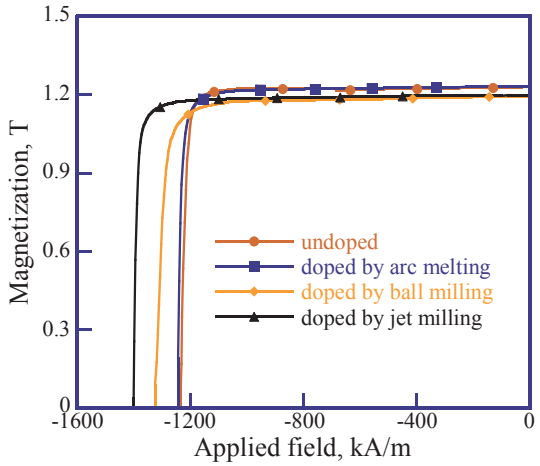

Fig. 3. The corresponding demagnetization curves for the magnets with pyrite doping by different methods.

Table 1
Composition of S and O elements in the pyrite-doped magnets fabricated by different doping methods.

Doping method	Undoped	Arc melting	Jet milling	Ball milling
S content (ppm)	138.4	105	2127.7	2267.5
O content (ppm)	4456.1	4466.8	4360.6	4371.1

4400 ppm). Although 0.38 w% FeS_2, nearly 0.2 wt% S, was added into the magnets, the S content for AMS magnets was only 105 ppm, compared to above 2000 ppm for the BMS and JMS magnets. From this, it can be inferred that there exists a loss of S element during the arc melting process. It has been reported that pyrite would decompose into Fe and S_2, under an anaerobic atmosphere at high temperature, as shown in formula (1) [19]:

$$FeS_2 \rightarrow Fe(s) + S_2(g) \quad (1)$$

When pyrite was doped in the magnets by arc melting at 1773 K, the pyrite would undergo chemical reaction immediately, resulting in the volatilizing of S element. Thus, the S content of AMS magnets is almost the same with that of the undoped magnets, which may be the impurities in raw materials. The volatilizing of the S element may be the main reason that the coercivity can't get enhanced when pyrite is doped by arc melting, as shown in Fig. 3.

The introduction of S element in the BMS and JMS magnets may change the structure of grain boundaries, or optimize the grain size distribution, resulting in the coercivity enhancement. To understand the relationship between microstructure and magnetic performance of the magnets, FESEM and EPMA investigations were conducted.

Fig. 4 shows the microstructure changes and grain size distribution in the magnets. The dark gray regions correspond to the $Nd_2Fe_{14}B$ main phases, and the bright regions correspond to the Nd-rich phases. Without pyrite addition, the grain boundary phases (GBPs) were fuzzy and discontinuous, and the grain size was relatively large, as shown in Fig. 4(a). The average grain size was 9.1 μm. Compared to the undoped magnets, clear and continuous GBPs were formed in the pyrite-doped magnets. Additionally, the grain size was relatively small and the grain size distribution was more uniform, as shown in Fig. 4(b) and (c). The average grain size for BMS magnets was 7.9 μm, while that for the JMS magnets was 6.7 μm. It is emphasized that the grain growth gets inhibited with pyrite addition. As a result, the coercivity of the magnets gets enhanced. Although equal amounts of pyrite were added, the average grain size and grain size distribution were different in BMS and JMS magnets. The average grain size for the JMS magnets is approximately 1.2 μm smaller than that of the BMS magnets, resulting in the higher coercivity in JMS magnets.

The distribution of Nd, O and S elements in the S-doped magnets fabricated by different doping method is shown in Fig. 5. It can be observed that the dominant components are Nd and O elements of the triple junction phases(TJPs). The crystal structures of Nd-rich phases are complex, consisting of dhcp-Nd, fcc-NdO_x, and hcp-Nd_2O_3 [20]. The distribution of S element in BMS magnets was not uniform with obvious clusters of S, as shown in Fig. 5(a). In contrast, the distribution of S element was relatively uniform in the JMS magnets. The S distribution was strictly overlapped with Nd and O distributions. It suggests that jet milling is an effective way to settle the problem of S aggregation with pyrite doping.

To identify the S-rich phase in the JMS magnets, TEM analysis was performed. Region "A" and "B" are in different locations at the triple junctions. From the EDS patterns, both region "A" and "B" are corresponding to the S-rich phase. The SAED patterns revealed that regions "A" corresponded to the Nd_2O_2S phase with a = 0.395 nm, and c = 0.679 nm, as shown in Fig. 6(a). The measured distances from (0 0 0) to (0 0 2), (1 1 0) were 0.329 nm and 0.197 nm, respectively. The zone axis was identified as $[\bar{1}10]$. Similarly, another SAED pattern

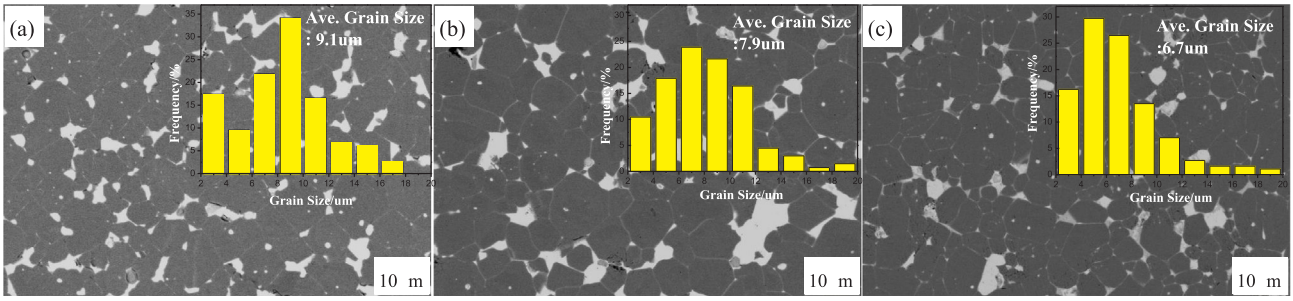

Fig. 4. SEM images and grain size distribution of: (a) undoped magnets, and S-doped magnets by (b) ball milling and (c) jet milling.

revealed that the S-rich phase in region "B" was also corresponding to hexagonal Nd_2O_2S phase. The distances from (0 0 0) to (0 1 1), (101) were 0.305 nm and 0.298 nm, respectively. The zone axis was identified as [111]. Although Al and Cu elements are present, the main S-containing precipitates are Nd_2O_2S phases in the magnets [17–18].

Fig. 7 presents the DSC curves of undoped and pyrite-doped magnets. The DSC analysis was carried out from room temperature to 1323 K, at a constant heating rate of 0.67 K/s. Two exothermic peaks are observed. The first peak, T_{x1}, is corresponding to the Curie temperature of the $Nd_2Fe_{14}B$ phase. In the pyrite-doped magnets, T_{x1} is about 600 K, almost the same as the undoped magnets. However, there is an obvious difference in T_{x2}, which corresponds to the melting point of the Nd-rich eutectic phase. T_{x2} was about 1038 K for the CS magnets. With 0.38 wt% pyrite addition, the melting point, T_{x2}, decreased to 1021 K. The melting point of Nd-rich eutectic phases, also known as the liquidus temperature, plays a key role in improving the wettability between the main phases and the Nd-rich phases. With pyrite addition, the melting point was lower than that of the CS magnets by 17 K, as seen in Fig. 7.

The above results indicate that S element plays a positive role on the GBPs optimization and grain inhibition in the Nd-Fe-B sintered magnets. Due to the reduction of the melting point, the wettability improves, resulting in the uniformity and continuity of GBPs [21]. The continuity of Nd-rich GBPs was improved in the pyrite-doped magnets, as shown in Fig. 4(b). The liquid Nd-rich phases in the TJPs were pulled into the grain boundaries through the capillary effect during sintering. Since the melting point of the Nd-rich phase decreased with S element addition, the wettability of the liquid Nd-rich phase, which was the driving force for the capillary action, was enhanced. In addition, the average grain sizes were optimized in the S-containing magnets. Therefore, the coercivity of BMS magnets were enhanced, 7.3% higher than that of the CS magnets. But one problem with the BMS magnets was that the distribution of S element was nonuniform. When it was doped by jet milling, the beneficial effects of S element would become more apparent, as shown in Fig. 3. With the uniform distribution of the S element, a finer grain size can be obtained, as shown in Fig. 4(c). The average grain size decreased from 9.1 μm to 6.7 μm. Consequently, the coercivity of the JMS magnets was 13.4% higher than that of the CS magnets.

4. Conclusions

In summary, the microstructure and magnetic properties of the pyrite-containing magnets doped by different methods were characterized. When pyrite was doped by arc-melting, the volatilizing of S element happened, resulting in no notable changes in the magnetic performance. When doped by jet milling, the coercivity reached its maximum, 13.4% higher than the undoped magnets. The melting point was decreased with pyrite addition, resulting in the GBPs optimization and grain refinement. Clear and continuous GBPs were formed and the average grain size decreased from 9.1 μm to 6.7 μm. Compared to the magnets with pyrite doped by ball milling, the distribution of S element in the magnets fabricated by jet milling was more uniform, with no S clusters existing at TJPs. Jet milling is an effective way to solve the uniformity problem of S distribution.

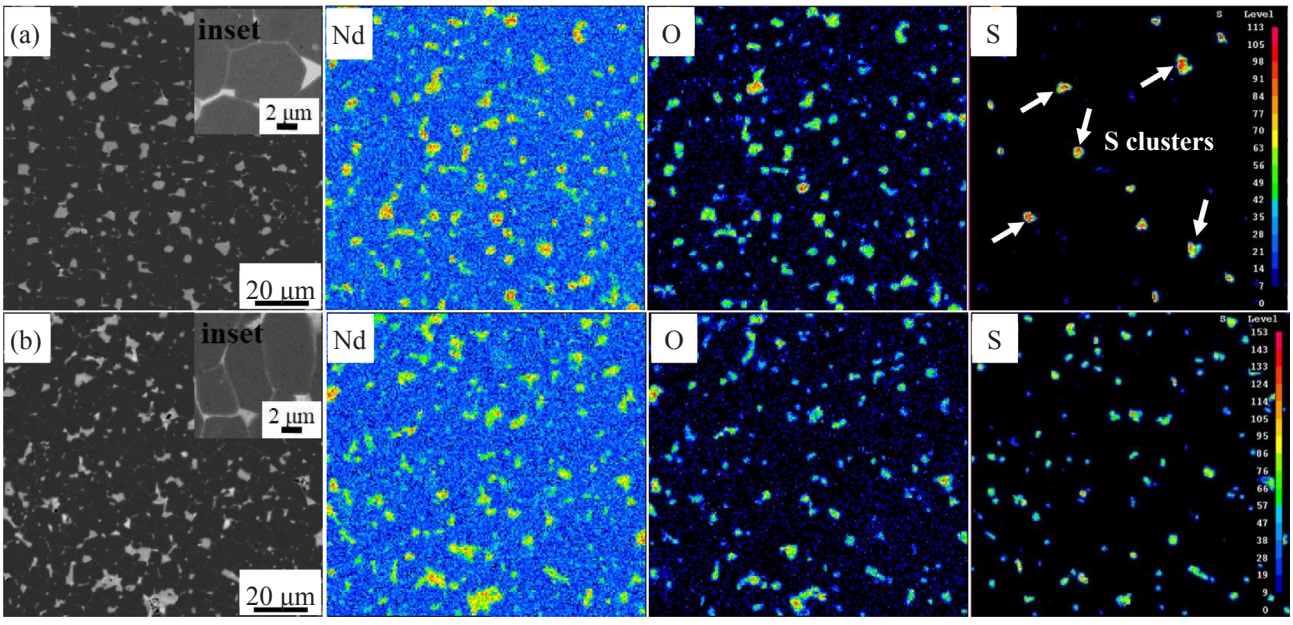

Fig. 5. EPMA maps of Nd, O and S elements of the S-doped magnets by (a) ball milling and (b) jet milling.

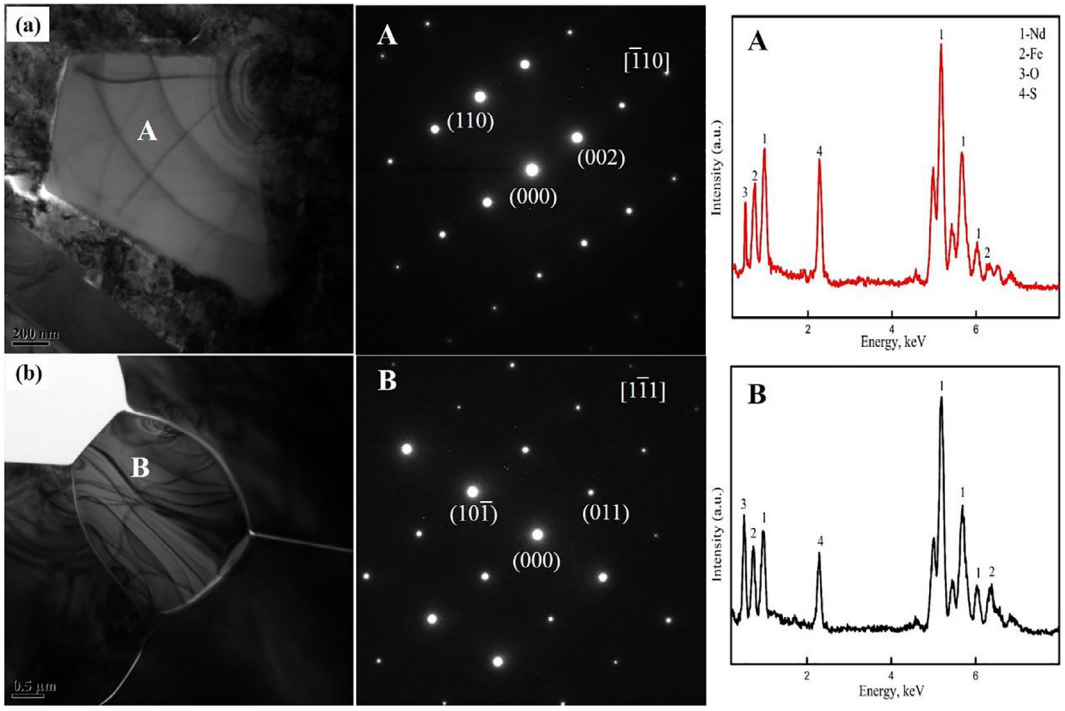

Fig. 6. TEM images, SAED and EDS patterns from region: (a) A, and (b) B in the magnets with pyrite doped by jet milling.

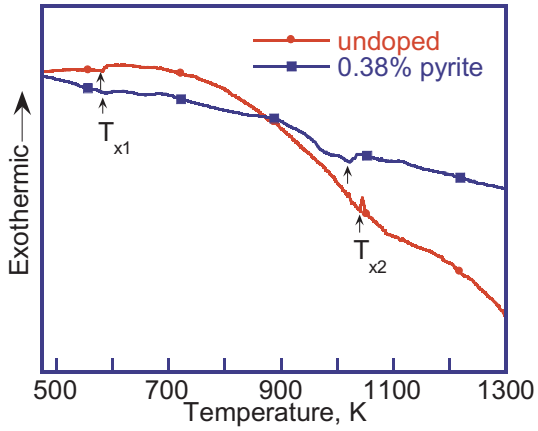

Fig. 7. DSC curves of the undoped and pyrite-doped magnets.

Acknowledgment

This work was supported by State Key Lab of Advanced Metals and Materials, China (No. 2018-Z06).

Appendix A. Supplementary data

Supplementary data associated with this article can be found, in the online version, at https://doi.org/10.1016/j.jmmm.2018.08.057.

References

[1] K. Hono, H. Sepehri-Amin, Strategy for high-coercivity Nd-Fe-B magnets, Scrip. Mater. 67 (2012) 530–535.
[2] K. Loewe, C. Brombacher, M. Katter, O. Guttfleisch, Temperature-dependent Dy diffusion processes in Nd-Fe-B permanent magnets, Acta Mater. 83 (2015) 248–255.
[3] J. Liu, H. Sepehri-Amin, T. Ohkubo, K. Hioki, A. Hattori, T. Schrefl, K. Hono, Effect of Nd content on the microstructure and coercivity of hot-deformed Nd-Fe-B permanent magnets, Acta Mater. 82 (2015) 336–343.
[4] Z. Mural, L. Kollo, M. Xia, C.R.H. Bahl, A.B. Abrahamsen, H.N. Bez, J. Link, R. Veinthal, The effect of nano-TiC addition on sintered Nd-Fe-B permanent magnets, J. Magn. Magn. Mater. 429 (2017) 23–28.
[5] F. Bittner, T.G. Woodcock, L. Schultz, S. Schwobel, O. Gutfleisch, G.A. Zickler, J. Fidler, K. Ustuner, M. Katter, Normal and abnormal grain growth in fine-grained Nd-Fe-B sintered magnets prepared from He jet milled powders, J. Magn. Magn. Mater. 426 (2017) 698–707.
[6] S. Bance, J. Fischbacher, T. Schrefl, Thermally activated coercivity in core-shell permanent magnets, J. Appl. Phys. 117 (2015) 17A733.
[7] T.T. Sasaki, T. Ohkubo, K. Hono, Structure and chemical compositions of the grain boundary phase in Nd-Fe-B sintered magnets, Acta Mater. 115 (2016) 269–277.
[8] W.F. Li, T. Ohkubo, K. Hono, Effect of post-sinter annealing on the coercivity and microstructure of Nd-Fe-B permanent magnets, Acta Mater. 57 (2009) 1337–1346.
[9] T.G. Woodcock, Y. Zhang, G. Hrkac, G. Ciuta, N.M. Dempsey, T. Schrefl, O. Gutfleisch, D. Givord, Understanding the microstructure and coercivity of high performance NdFeB-based magnets, Scrip. Mater. 67 (2012) 536–541.
[10] J.W. Kin, W.S. Lee, J.M. Byun, S.H. Kim, Y.D. Kim, Grain refinement in heavy rare earth element-free sintered Nd-Fe-B magnets by addition of a small amount of molybdenum, J. Appl. Phys. 117 (2015) 17B523.
[11] W.H. Cheng, W. Li, C.J. Li, X.M. Li, The role of Nb addition in Nd-Fe-B sintered magnets with high performance, J. Alloy Compd. 319 (2001) 280–282.
[12] T.Y. Chu, T.S. Chin, C.H. Lin, J.M. Yao, Evidence of domin-wall pining in W-doped (NdDy)(FeCo)B sintered magnets, J. Appl. Phys. 76 (1994) 6834.
[13] S. Pandian, V. Chandrasekaran, G. Markandeyulu, K.J.L. Lyer, K.V.S. Rama-Rao, Effeet of Al, Cu, Ga, and Nb additions on the magnetic properties and microstructural features of sintered NdFeB, J. Appl. Phys. 92 (2002) 6082–6086.
[14] H.J. Engelmann, A.S. Kim, G. Thomas, Microstructure and magnetic effects of small Cu additions to (Nd, Dy)FeB magnets, Scrip. Mater. 36 (1997) 55–62.
[15] W.F. Li, A.M. Gabay, M. Marinescu-Jasinski, J.F. Liu, C. Ni, G.C. Hadjipanayis, Microstructure of sintered ND-Fe-Ga-B magnets with Mo and MoS_2 addition, J. Magn. Magn. Mater. 324 (2012) 1391–1396.
[16] K.H. Bae, S.R. Lee, H.J. Kim, M.W. Lee, T.S. Jang, Effect of WS_2/Al co-doping on microstructural and magnetic properties of Nd-Fe-B sintered magnets, J. Alloys Compd. 673 (2016) 321–326.
[17] A.M. Gabay, M. Marinescu, W.F. Li, J.F. Liu, G.C. Hadjipanayis, Dysprosium-saving improvement of coercivity in Nd-Fe-B sintered magnets by Dy_2S_3 additions, J. Appl. Phys. 109 (2011) 083916.
[18] F. Yang, L.C. Guo, P. Li, X.Z. Zhao, Y.L. Sui, Z.M. Guo, X.X. Gao, Boundary structure modification and magnetic properties of Nd-Fe-B sintered magnets by co-doping with Dy_2O_3/S powders, J. Magn. Magn. Mater. 429 (2017) 117–123.
[19] R.C. Sharma, Y.A. Chang, Thermodynamics and phase relationships of transition metal-sulfur systems: thermodynamic properties of the Fe-S liquid phase and the calculation of the Fe-S phase diagram, Metall. Mater. Trans. B 10 (1979) 103–108.
[20] T.G. Woodcock, O. Gutfleisch, Multi-phase EBSD mapping and local texture analysis in Nd-Fe-B sintered magnets, Acta Mater. 59 (2011) 1026–1036.
[21] T.H. Kim, S.R. Lee, M.W. Lee, T.S. Jang, J.W. Kim, Y.D. Kim, H.J. Kim, Dependence of magnetic, phase-transformation and microstructural characteristics on the Cu content of Nd-Fe-B sintered magnets, Acta Mater. 66 (2014) 12–21.